

Impact of 3D Printing Infill Patterns on the Effective Permittivity of 3D Printed Substrates

JEEVAN PERSAD  (Member, IEEE) AND SEAN ROCKE  (Senior Member, IEEE)

(Regular Paper)

Department of Electrical and Computer Engineering, The University of The West Indies, Saint Augustine, Trinidad and Tobago

CORRESPONDING AUTHOR: Jeevan Persad (e-mail: jeevan.persad@sta.uwi.edu).

ABSTRACT 3D printing can potentially transform traditional electronics manufacturing by allowing for the accurate direct digital manufacture of complex electronic structures with a much smaller process footprint. However, there are challenges which restrict the use of 3D printing for electronic manufacturing. One significant challenge is the characterization of the electromagnetic properties of the 3D printed materials such as their resultant dielectric permittivity. This work reports on the investigation of existing mixture models to establish their suitability for predicting the dielectric permittivity of 3D printed binary materials for the test frequency range of 1 GHz to 10 GHz. The identified models included volume fraction mixture models which considered the material volume concentration of the binary material and shape factor mixture models which consider the geometry and distribution of the mixture constituents. The fused filament fabrication 3D printing process was used for this work. 3D printed samples were produced with varying percentage volume compositions and varying infill patterns. The dielectric permittivity of the samples was investigated using the two-layer stripline measurement method and the measured data compared to the mixture model estimates. The shape factor mixture models were found to not be in good agreement with the measured values of dielectric permittivity. This result was attributed to the relatively small size of the discontinuities within the 3D printed substrate being insufficient to present anisotropy relative to the wavelength of the applied test signals. The volume fraction models were found to be in close agreement for samples with select infill patterns.

INDEX TERMS Mixture models, 3D-printing, additive manufacturing, dielectrics, material characterization.

I. INTRODUCTION

The present global geopolitical climate continues to contribute to a rapid pace of change which has significant impact on supply chains and in particular the supply of electronics goods and services [1]. In response, many stakeholders have begun rethinking the electronics ecosystem including the reshoring of electronics manufacturing and related research and development (R&D) capacity [2]. This prevailing climate presents an opportunity for the reimaging of the role of 3D printed (3DP) electronics as applied to R&D and application. 3D printing has enjoyed significant application to manufacturing and development of various electrical structures including active & passive components, antennas, sensors, and waveguides [3]. Based on the reported literature, the dominant 3D printing processes which have been applied to electrical applications include fused filament fabrication (FFF) which is a form of material extrusion, stereolithography (SLA) and

material jetting (MJT) [3]. Significant progress has also been made in the realization of systems capable of producing complete printed circuit assemblies (PCAs) [4].

Despite the tremendous progress made and wide array of application, there is still work to be done toward the characterization of 3DP materials [5]. 3DP materials are often preprocessed into different forms suited to the particular 3D printing process for example liquid and gel suspensions of nanoparticles, material pellets, and filaments [3]. The reconstituted materials which are produced as part of the 3DP object often possess differing characteristics when compared to the equivalent bulk unprocessed materials. Examples of variations can include mechanical, such as structural strength and electromagnetic (EM), such as conductance, permittivity, and permeability. Variations can also be introduced based on factors directly related to the specific 3D printing process. An example of a 3D printing process factor which is related to

the FFF 3D printing process is the use of infill supports for the printed structure, specifically, the percentage density of the infill and the infill pattern. The choice of these parameters can introduce benefits to the 3DP electrical structure. For example, a specific infill pattern and density can provide improved strength along all three axes or conversely improved flexibility and also reduce overall weight or reduce the manufacturing time. There can also be localized changes to the EM properties, such as dielectric permittivity, due to the 3DP material mixture deposited at a particular area. Quantifying the resultant changes to the EM properties of the 3D printed electrical structures as a result of material and process specifications can allow for the production of 3DP electrical structures with known characteristics on demand.

The estimation of the EM characteristics of 3DP electrical structures can be undertaken using various methods including empirical studies and the use of mathematical material mixture models [6]. Material mixture models take into consideration various characteristics of the mixture constituents as well as the material mixture in order to estimate the resultant properties. An example of a characteristic would be the volume composition of each constituent material contained in the mixture. An example EM related resultant property of interest would be the effective permittivity of the material mixture. The identification/derivation of suitable mixture models which can allow for the accurate estimation of the EM properties of 3DP materials is necessary for the design and modeling of electrical structures which are intended to be manufacturing using 3D printing processes. The lack of accurate material modeling data can lead to wide variations between the designed and built application (for example a wearable sensor) leading to significant variation between the intended and actual performance of the device [7].

In this work we report on research conducted to evaluate the EM properties of 3DP material mixtures. The specific EM property which is evaluated is the resultant dielectric constant (ϵ_{eff}) of the material mixtures. The material mixtures considered are binary mixtures composed of the printer material and air. The study involved the evaluation of 3DP material mixture samples using a transmission line measurement method for the test frequency range of 1 GHz to 10 GHz [8]. The measured data was then compared against the estimated values of ϵ_{eff} as predicted using various mixture models. The measurement method was selected owing to the adaptability of the method for the rapid evaluation of a large number of samples and minimum need for machining of test samples [9]. The mixture models were selected based on various characteristics of the material mixture which were considered by the models. For this work, volume fraction mixture models and shape factor mixture models were considered. Furthermore, the 3DP samples which were prepared for this study were evaluated based on the volume fraction composition of the printer material and air as well as the pattern of the infill supports used in the printed structure. The dimensions of the various discontinuities within the infill patterns of the 3DP samples were quantified using a microscope and evaluated

against the wavelength of the applied signal. It was noted that none of the measured discontinuities were sufficiently large to cause the 3DP substrates to demonstrate any anisotropy relative to the wavelength of the applied test frequency band. It can be expected that for higher frequencies that the impact of the discontinuities would manifest as illustrated in similar studies of 3DP structures which considered higher applied signal frequencies [10], [11], [12]. The 3D printing technology selected for this work was FFF 3DP. The FFF process was selected owing to its significant use in the reported literature as well as its affordability and ease of operation [3]. The 3D printer material utilized for this work was polylactide (PLA). PLA was chosen because of its good compatibility with the FFF 3D printing process and the overall low environmental impact of the material when compared to similar polymer materials [13].

The remaining sections of this paper will provide a brief overview of the FFF 3D printing process (Section II) followed by an overview of material mixture models (Section III). Next, the characteristics of the 3DP material mixtures which are relevant to the choice of mixture models will be discussed and the mixture models which are examined in this work will be introduced (Section IV). Following this, the methodology adopted for the work will be described in detail including a description of the two-layer stripline measurement method (Section V). The results obtained from the work will be presented for both the empirical study and the estimates from the mixture models (Section VI). The results will then be discussed (Section VII). Finally, the paper will close with the conclusion (Section VIII) and recommendations for future work (Section IX).

II. OVERVIEW OF THE FFF 3D PRINTING PROCESS

The 3D printing technology selected for this work was fused filament fabrication (FFF). The FFF 3D printing technology is categorized as a material extrusion process as defined by the International Organization for Standardization (ISO) and the American Society for Testing and Materials (ASTM) [14]. The FFF 3D printing process is currently one of the most prevalent 3D printing technologies owing to the low procurement and operating cost of the equipment, the simplicity of the operating processes and the expiration of key technology patents which has led to a proliferation of equipment manufacturers [3].

The creation of a 3DP electrical structure using FFF 3D printing involves several steps. The process commences with the creation of a digital model of the desired 3DP structure using either 3D scanning equipment or a drawing produced using computer aided design (CAD) software. The digital model is then modified for printing on the FFF 3D printing equipment using a slicer software tool. The slicer software converts the digital model into a series of layers and embeds the FFF printer equipment settings as specified by the user.

The materials processed using FFF 3D printing are often continuous filaments of thermoplastics. The filament material is heated into a semifluid state using the printer extrusion

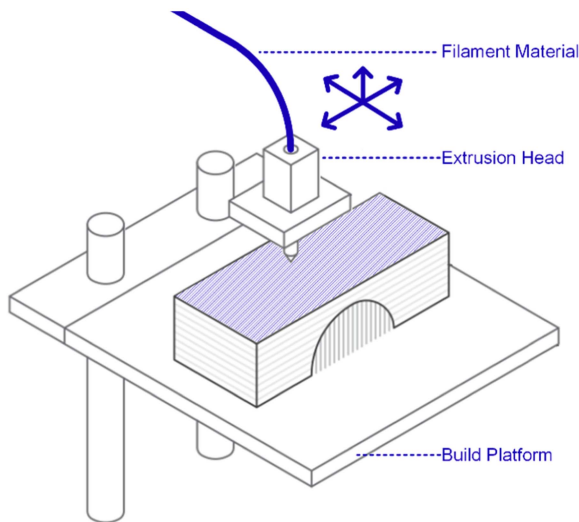


FIGURE 1. Simple diagram of the FFF 3D printing process.

nozzle. The nozzle is then precisely positioned using a gantry system and material is deposited in the desired location to build the 3DP object layer by layer. Bonding between layers is achieved through reptation of the semifluid material and underlying printed layers [4]. As previously stated, the filament material chosen for this work was polylactide (PLA). A simple diagram of the FFF 3D printing process is shown in Fig. 1.

III. OVERVIEW OF MATERIAL MIXTURE MODELS

One of the simplest FFF material mixtures is a composition of two materials (a binary mixture) where the constituent materials are air and the printer material (filament material). The ability of the material to impact the applied EM field is dependent on the mass of the material which interacts with the field [15]. There are several factors which can impact the resultant EM properties of the material mixture [16], [17], [18], [19]. These factors are illustrated in Fig. 2 and can be grouped into three general categories based on their nature: mechanical, environmental and electrical.

A. MECHANICAL FACTORS

There are several factors related to the mechanical/physical properties of the constituent materials contained in the mixture. The physical properties can include the physical state of the constituents (solid, liquid, gaseous etc.), the number of different constituents and the geometric arrangement/distribution of the constituents. The geometry/shape of the individual constituents as well as the boundary between the individual materials (chemical interphase and interface) are also important factors [15], [16], [18], [19]. There are several quantifying factors that are related to the constituents these include the concentration of the constituents and the bulk density of the overall mixture as well as the individual constituents [18]. Many derived models for material mixtures hold well for low concentrations of the inclusion material [16]. One phenomenon that contributes to the deviation of the mixture

models is the occurrence of percolation within the material mixture. Percolation occurs when disparate clusters of similar materials become interconnected forming a contiguous chain. In some cases, the contiguous chains can permeate across the entire body of the dielectric structure [16]. The occurrence of percolation is dependent on several mechanical and electrical properties of the materials. The mechanical related factors include the material concentrations, physical state, distribution pattern, bulk density and the size and shape of the material inclusions. Therefore, it can be appreciated that percolation can occur at relatively low concentrations in systems with a disordered distribution. The electrical factors which impact percolation include the EM field that is acting on the dielectric structure and the EM properties of the materials. Finally, when including mechanical/physical factors, consideration must be given to the degree of deformation and/or strain which the dielectric structure is subjected to [20].

B. ENVIRONMENTAL FACTORS

The overall environment impacting the mixture and its constituents can also have implications on the resultant dielectric permittivity of the dielectric structure. Relevant environmental factors include the temperature and humidity surrounding the mixture. The environmental conditions are also important when one considers the aging of the 3DP dielectric structure and the consequent changes to the resultant dielectric permittivity of the individual constituents and by extension the overall material mixture.

C. ELECTRICAL FACTORS

There are several important electrical related properties of the mixture constituents and the overall operating conditions that can impact the resultant dielectric permittivity of the dielectric structure. The first significant factor is the EM properties of the individual constituents (conductivity, permittivity, permeability etc.). Also of importance is the nature of the EM wave which is applied to the dielectric structure, this includes the amplitude and frequency of the applied signal [16], [17], [18]. A significant EM property of the constituents which is related to the frequency of the applied signal is the polarization of the materials. Polarization provides a measure of a material's ability to capture and release electric and magnetic energy [21]. Polarization can be expressed in terms of the dielectric susceptibility of the material and the applied electric field [22]. Polarization can be considered at a micro and macro scale including deformation polarization at the atomic level, orientation polarization at the molecular level and ionic polarization at the lattice level [23]. In some instances, a material may possess a permanent displacement of charge at the molecular level (without the application of an electric field). This charge displacement is known as a dipole moment. Material mixtures which contain at least one material with dipoles is referred to as a polar mixture. Conversely a nonpolar mixture experiences a dipole moment only when the electric field is applied.

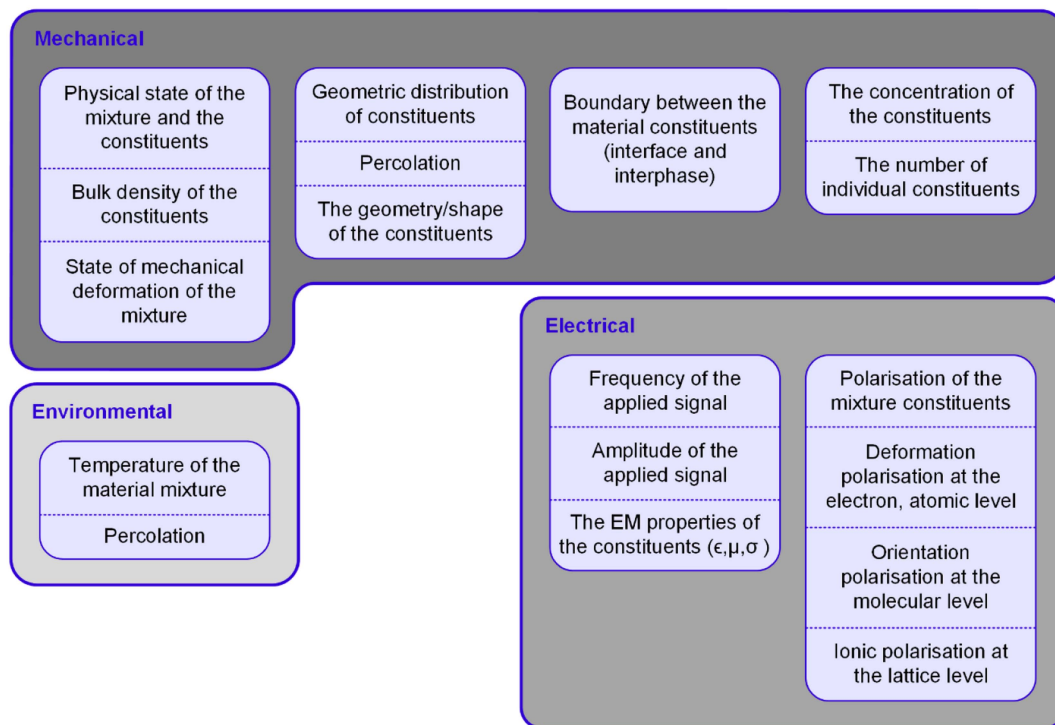


FIGURE 2. Various factors that can impact the resultant EM properties of a material mixture.

D. CATEGORIES OF MIXTURE MODELS

Historically, mixture models have been derived as a means to estimate the EM properties of material mixtures such as the resultant dielectric constant (ϵ_{eff}). As previously discussed, the EM properties of a material mixture are affected by a number of factors. Mixture models can be grouped based on the specific factor(s) considered by the models. For this reported work, mixture models which consider the volume composition of the material mixture (volume fraction models) and models which consider the geometry of the constituents (shape factor models) were used for the evaluation of the 3DP samples.

Volume fraction mixture models consider the volume fraction q_i of each component within the mixture [19].

$$q_i = \frac{(m_2 \rho_2)}{(m_2 \rho_2 + m_1 \rho_1)} \tag{1}$$

where m_1 is the matrix weight, m_2 is the weight of inclusions, ρ_1 is the matrix density, ρ_2 is the inclusion density. It is important to note that there is a limit to how densely material can be packed based on the size of inclusions and cohesion forces between particles and in many cases a 100% packing volume is not realistic [6]. This is particularly relevant for the FFF 3D printing process where the 3DP structure is constructed from a series of extruded contiguous material fibres with associated airgaps between the tightly packed strands. Shape factor mixture models give consideration to the shape of the inclusion contained within the material mixture by including a shape factor in their expression.

IV. RELEVANT CHARACTERISTICS OF THE FFF 3D PRINTING PROCESS

As discussed previously, the choice of mixture models for the evaluation of a material mixture is dependent on the factors which are considered relevant for the material mixture. Establishing which factors are relevant would depend on the nature of the material mixture. Some examples of relevant factors would include: volume composition of the materials, whether the material mixture is homogenous/non-homogenous, whether constituents are lossy materials. The characteristics of the 3DP material would also be dependent on the 3D printing parameters relevant to the 3D printing process. Some examples of printing parameters would include: the percentage infill (%infill) utilized for the printing of the electrical structures, the width of the print layers (walls, shells and infill supports).

For this work several key assumptions were made which influenced the choice of mixture models. These assumptions are as follows:

- The physical state of the 3DP polymer material (PLA) is solid and for this work the idealized complex permittivity of air will be considered to be $1 - j0$.
- The PLA material used for this work is considered to be a non-polar material. The dispersion effects of the material are considered to be negligible, losses within the material are negligible and the relative permeability of the material $\mu_r = 1$.
- Air gaps in the 3DP structure are an artefact of the printing process. For FFF printing the air gaps can exist as

imperfections between the printed material lines or as part of the infill pattern that is specified for the 3DP part.

Based on the above assumptions the various mixture models were identified for evaluation.

A. VOLUME FRACTION MIXTURE MODELS

The 3DP material mixtures are considered to be composed of two distinct materials, namely, air, and PLA. Volume fraction mixture models were identified which estimated the resultant dielectric constant (ϵ_{eff}) based on the volume (v_1, v_2) and the dielectric constant (ϵ_1, ϵ_2) of the constituents. The mixture models selected were Landau & Lifshitz, Looyenga (LLL), Refractive Index (RI), Lichtenecker (LI), Rayleigh (RAY) and Böttcher (BOT).

1) LANDAU & LIFSHITZ, LOOYENGA (LLL)

The model considers a cubic root relationship between the dielectric constant of the constituents and the resultant dielectric constant [24]. This type of mixture model is also categorized as a power law model [25]:

$$(\epsilon_{eff})^{1/3} = v_1(\epsilon_1)^{1/3} + v_2(\epsilon_2)^{1/3} \quad (2)$$

2) REFRACTIVE INDEX (RI)

The model is another example of a power law model. A squared root relationship is described for ϵ_{eff} [15]. The model is also known as the Birchak model or Beer model [26], [27]:

$$(\epsilon_{eff})^{1/2} = v_1(\epsilon_1)^{1/2} + v_2(\epsilon_2)^{1/2} \quad (3)$$

3) LICHTENECKER (LI)

The model describes a logarithmic association between the dielectric constant of the constituents and the value of ϵ_{eff} [28]:

$$\ln \epsilon_{eff} = v_1 \ln \epsilon_1 + v_2 \ln \epsilon_2 \quad (4)$$

4) RAYLEIGH (RAY)

The RAY model considers the material mixture to be composed of two dielectric materials one of which is the inclusion material and the other is the matrix material contained within a unit cell [29]. The expression is also referred to as the Maxwell Garnett equation [30]:

$$\frac{\epsilon_{eff} - \epsilon_1}{\epsilon_{eff} + 2\epsilon_1} = v_2 \frac{\epsilon_2 - \epsilon_1}{2\epsilon_1 + \epsilon_2} \quad (5)$$

5) BÖTTCHER (BOT)

The BOT model considers an inclusion which is a spherical particle with an associated electric field that is contained within a matrix material [31]:

$$\frac{\epsilon_{eff} - \epsilon_1}{3\epsilon_{eff}} = v_2 \frac{\epsilon_2 - \epsilon_1}{\epsilon_2 + 2\epsilon_{eff}} \quad (6)$$

B. SHAPE FACTOR MIXTURE MODELS

The shape factor mixture models chosen for this work were identified based on considerations of the geometric details of the 3DP material mixture. Of particular importance was the

shape, size, and distribution of the discontinuities within the 3DP material structure. The relevance of a geometric feature to the EM properties of the 3DP material mixtures is dependent on the relationship between the wavelength of the applied signal (λ) and the size of the inclusions or any discontinuities in the mixture structure (ξ_i) [16], [17], [32]. A discontinuity can be considered to have negligible potential to impact the field of the applied signal for the following condition

$$k_i \xi_i \ll 1 \quad (7)$$

where ξ_i is the size of each different discontinuity within the material and k_i is dependent on the properties of the inclusion and matrix material in the material mixture such that [33]:

$$k_i = \frac{2\pi}{\lambda} \cdot (\epsilon_i \mu_i)^{1/2} \quad i = 1, 2 \quad (8)$$

For this work, the 3DP material mixtures are considered to be composed of PLA and air. Therefore, the subscripts 1 and 2 denote the inclusion material (air) and the matrix material (PLA) and ϵ_i and μ_i are the relative permittivity and permeability of the materials respectively. Once the condition is met, the impact of any discontinuities within the substrate can be ignored and the 3DP substrate can be considered to be homogenous for the applied field.

As stated previously, the permeability of the inclusion and matrix material are assumed to be 1. The frequency range of the applied signal is 1 GHz to 10 GHz which corresponds to a wavelength λ of 0.30 m to 0.03 m then:

- the range of k_1 for $\epsilon_1 = 1.00$ (air) is 20.94 m⁻¹ to 209.44 m⁻¹
- the range of k_2 for $\epsilon_2 = 2.75$ (PLA) [34] is 34.73 m⁻¹ to 347.32 m⁻¹

Using the range of values for k_1 and k_2 the various discontinuities within the 3DP structure can be evaluated based on expression (7) to establish whether each discontinuity would impact the applied signal and must be considered by the mixture model. For this work, the various discontinuities ξ_i of the 3DP materials were quantified using a microscope and is described later in this report. Based on the result of the evaluation the Sillars & Fricke (SF) and Emets (EMT) shape factor mixture models were selected.

1) SILLARS & FRICKE (SF)

The Sillars model is an example of a mean field theory (MFT) mixture model also known as the effective medium approach. The Sillars model was further considered by Sillar and Fricke (SF) in order to account for higher concentrations of inclusions. Steeman [35] also considered the instance where the matrix material was conductive in nature. The SF model considered ellipsoidal shaped inclusions contained within a matrix material. The different ellipsoidal shapes (dependent on the direction of the applied electric field) are assigned a shape factor. Examples of general shape categories include disks, cylinders, needles and spheres. The expression for resultant

dielectric constant for the SF model is given by [36], [37]:

$$\epsilon_{eff} = \frac{\epsilon_1 (\eta \epsilon_2 + (1 - \eta) \epsilon_1) - v_2 (1 - \eta) (\epsilon_2 - \epsilon_1)}{(\eta \epsilon_2 + (1 - \eta) \epsilon_1) - \eta v_2 (\epsilon_2 - \epsilon_1)} \quad (9)$$

where ϵ_1 is the dielectric constant of the matrix material, ϵ_2 is the dielectric constant of the inclusion material, v_2 is the volume fraction of inclusion material, η is the inverse of the shape factor n . The shape factor is related to the direction of the electric field and the ellipsoidal axes:

$$n_i = \frac{2}{x_1 x_2 x_3 \mathcal{L}_i} \quad (10)$$

where i is the axis direction $i = \{1, 2, 3\}$, $x_1 x_2 x_3$ are the radii of the ellipsoid in the directions 1,2,3. \mathcal{L}_i is given by:

$$\mathcal{L}_i = \int_0^\infty \frac{d\zeta}{\left[(x_i^2 + \zeta)^2 (x_1^2 + \zeta) (x_2^2 + \zeta) (x_3^2 + \zeta) \right]^{1/2}} \quad (11)$$

where ζ is an integration variable and the value of \mathcal{L}_i is between 1 and ∞ . The shape factor, n for needle like inclusions is >3 and n is 3 for spherical inclusions. For cylindrical inclusions perpendicular to the applied field n is 2 and for large discs perpendicular to the field, n is 1.

For the FFF manufactured PLA dielectric materials, the SF was considered for the condition where the applied field is impacted by the contiguous printed lines of PLA material. The two extreme conditions would be the applied electric field incident to the PLA cylinders perpendicularly (cylinder of infinite length) and incident to the cylinder (disc). For the incident applied field, $n = 1$ and the expression for ϵ_{eff} is given by (SF-Inc):

$$\epsilon_{eff} = \frac{\epsilon_1 \epsilon_2}{\epsilon_2 - v_2 (\epsilon_2 - \epsilon_1)} \quad (12)$$

For the perpendicular applied field, $n = 2$ and the expression for ϵ_{eff} is given by (SF-Per):

$$\epsilon_{eff} = \frac{1}{2} \left(\frac{\epsilon_1 (\epsilon_2 + \epsilon_1) - v_2 (\epsilon_2 - \epsilon_1)}{(\epsilon_2 + \epsilon_1) - v_2 (\epsilon_2 - \epsilon_1)} \right) \quad (13)$$

2) EMETS (EMT)

The Emets mixture model was developed to consider inclusions in the form of tightly packed cylindrical fibre material in a matrix material. The packing pattern is considered to be a periodic lattice with doubly periodic cylinders of radii r_1 and r_2 respectively. By extension, the material mixture is assumed to be composed of two fibre materials and the matrix material where ϵ_1 , ϵ_2 , ϵ_3 are the dielectric constant of the cylinder 1, cylinder 2 and the matrix material respectively [38]. For the FFF 3D printed material mixtures the fibres can be considered to be PLA cylinders of the extruded material. Thus, the assumption can be made that $r_1 = r_2$ and $\epsilon_1 = \epsilon_2$ and the expression for ϵ_{eff} would be given by:

$$\epsilon_{eff} = \epsilon_1 \frac{1 - \frac{\Delta_{13} v_1}{2} + A \Delta_{13}^2}{1 + \frac{\Delta_{13} v_1}{2} + A \Delta_{13}^2} \quad (14)$$

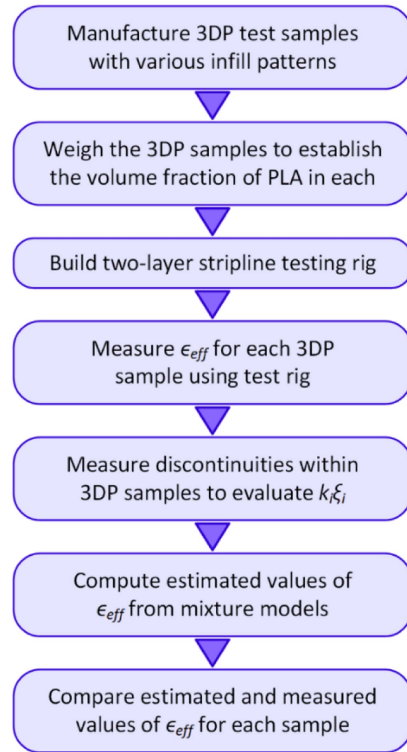


FIGURE 3. Methodology adopted for this work.

where Δ_{13} is given by

$$\Delta_{13} = \frac{\epsilon_1 - \epsilon_3}{\epsilon_1 + \epsilon_3} \quad (15)$$

and A is a function of the radius of the cylinders = 0.09644.

V. METHODOLOGY

This work involves an empirical study to examine the resultant dielectric constant (ϵ_{eff}) of 3DP binary material mixtures with varying infill patterns and the resultant varying volume compositions of the composite materials. The composite materials are air and PLA. A transmission line method of measurement was adopted for the evaluation of the 3DP samples. The measured data was then compared to the predicted values of ϵ_{eff} for various volume fraction and shape factor mixture models. The methodology adopted for this work is illustrated in Fig. 3 and will be described in detail in this section of the reported work.

A. PREPARATION OF 3DP SAMPLES

A previously reported examination of the literature was conducted to identify a suitable 3DP electrical structure for the empirical analysis [3]. Several categories of electrical structures were identified and a simple geometric dielectric structure was finally selected. The dielectric structure was chosen since it can be easily produced as a simple geometry (most common shape being a cuboid) which is desirable when undertaking the measurements of ϵ_{eff} . In addition, the

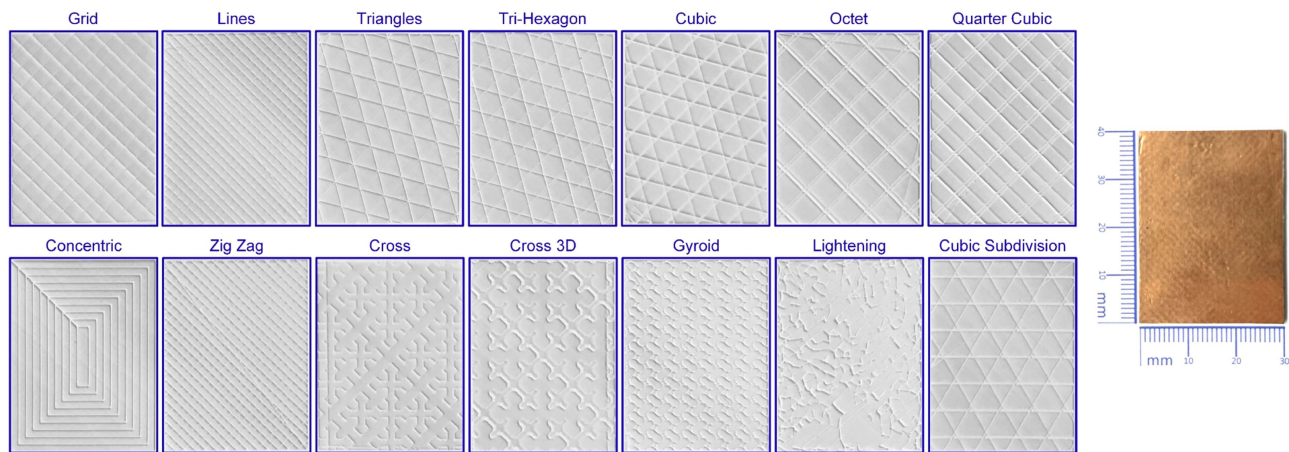


FIGURE 4. Details of the various infill patterns used for the FFF 3DP samples produced with varying infill patterns.

reported dielectric work in the literature made significant use of the FFF printing technology which was selected for this study. The FFF samples were produced using existing inhouse equipment, the specific 3D printing equipment was the Ender3 FFF printer. For this work, the dimensions of the geometry of the 3DP dielectric structure were designed to be comparable with a standard dielectric structure commonly used in the manufacture of conventional electronics using traditional photolithographic manufacturing processes (traditional subtractive manufacturing processes). The traditional structure chosen was a standard, rigid Printed Circuit Board (PCB), Flame Retardant 4 (FR4) laminate [39].

The software used for the creation of the CAD file of the dielectric structure was the COMSOL Multiphysics software. The CAD file was exported in .stl format from the COMSOL software. The .stl format is widely compatible with many Computer Aided Manufacturing (CAM) platforms such as 3D printing applications. Additional processing of the .stl file is required before it can be used with the 3D printer equipment. The processing of the .stl file results in the generation of an equivalent Computer Numerical Control (CNC) format. The CNC format commonly utilized by the 3D printer equipment is the g-code format. The process of converting the .stl file into the equivalent g-code format is known as slicing. Slicing involves converting the CAD drawing into a series of layers as well as the tool path for the printing. The software used for the slicing was the open source Cura slicing software [40].

The 3DP dielectric structures were all manufactured with the same outer dimensions of 30 mm × 40 mm × 0.8 mm with varying infill patterns. The infill patterns used for the research were generated using the Cura slicer software and the %infill was maintained at 10% for all patterns. All other 3D printing parameters were kept constant for all the samples. The print resolution of the FFF 3D printer was 0.1 mm in all three axes and the diameter of the extrusion nozzle used for the printing was 0.2 mm. In total fourteen infill patterns were used for the research. A set of ten 3DP samples were produced for each infill pattern. The weight of each 3DP

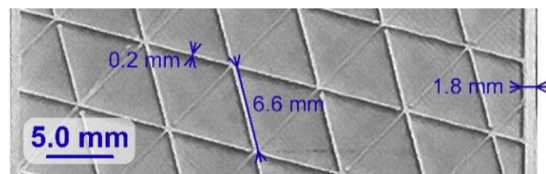


FIGURE 5. Example measurements of discontinuities within the 3DP structure for the triangle infill pattern.

sample was measured and the volume fraction of the PLA and air was calculated using (1) and the density of the PLA material as specified by the materials supplier (1.27 g/cm^3) [41]. To complete the preparation of the samples for testing, each sample was outfitted with a copper ground plane using 1 oz, 3M 1125 copper foil as required for the two-layer stripline measurement method. The details of the infill patterns as well as a prepared 3DP sample with copper ground plane applied are shown in Fig. 4.

Finally, as stated previously, the discontinuities within the 3DP samples were measured in order to establish their size. The measured discontinuities were then evaluated using (7) to establish the state of homogeneity of the 3DP substrate. Fig. 5 illustrates an image of the measurements for the 3DP sample with triangle infill pattern (10% infill). The details measured included the outer shell ($\xi_1 = 1.8 \text{ mm}$), infill wall thickness (which is the same width of the individual print line) ($\xi_2 = 0.2 \text{ mm}$) and the side of the triangle infill ($\xi_3 = 6.6 \text{ mm}$). Table 1 summarises the calculated values of $k_i \xi_i$ for the example 3DP sample shown in Fig. 5 for the frequency range of 1 GHz to 10 GHz (λ of 0.30 m to 0.03 m). The values of k_1 (for air) and k_2 (for PLA) were previously calculated.

From the example results listed in Table 1 it is observed that expression (7) does not hold for various discontinuities especially at the higher frequencies. Therefore, the 3DP dielectric substrates cannot be considered as homogenous. It is for this reason that mixture models which give consideration to a shape factor were examined to establish their suitability

TABLE 1. Measured Values of ξ_i and the Calculated Values of $k_1\xi_3$ and $k_2\xi_{1,2}$ for the Triangle Infill Pattern

Discontinuity in the 3DP Substrate	Calculated $k_2\xi_{1,2}$ for λ (0.30 m – 0.03 m)
Outer shell top/bottom/sidewall width (0.0018 m) (ξ_1) Material is PLA	0.0625 to 0.6252
Individual print line width, and infill wall thickness (0.0002 m) (ξ_2) Material is PLA	0.0069 to 0.0695
	Calculated $k_1\xi_3$ for λ (0.30 m to 0.03 m)
Inner face of equilateral triangle infill pattern (0.0066 m) (ξ_3) for 10% infill Material is PLA	0.1385 to 1.3847

for predicting the values of resultant permittivity for the 3DP dielectric substrates.

B. TWO-LAYER STRIPLINE MEASUREMENT METHOD

The transmission line method was adopted for the evaluation of the ϵ_{eff} of the 3DP dielectric substrates. The method involves the introduction of the material under test (MUT) into the transmission line such that the applied signal is directed at the MUT sample [42], [43], [44]. The specific transmission line testing method used for this work was the two-layer stripline measurement method [9]. The stripline measurement method allows for the testing of a wide array of MUT sample dimensions with no machining of test samples required. Furthermore, samples can be quickly tested allowing for the rapid testing of a large number of samples. The method can be used with the intended frequency band of 1 GHz to 10 GHz adopted for this research and the reported accuracy of the test method is better than $\pm 1\%$ [9]. There are several assumptions which are applied when using the stripline measurement method:

- The transmission line width (w) is sufficient larger than the thickness of the dielectric material (H) such that $w/H \geq 1$. Once this condition is met it can be assumed that the dispersion effects of the field lines from the transmission line would be negligible.
- The dispersion effects of the dielectric material are negligible
- Losses within the dielectric are negligible and conductor losses are predominantly in the transmission line
- The relative magnetic permeability of the dielectric material is $\mu_r = 1$
- The propagation mode of the applied signal can be approximated to a transverse electromagnetic mode

The details of the measurement setup will now be described.

1) OPERATIONAL THEORY

The two-layer stripline measurement method involves the use of a 50 ohm microstrip line constructed on a known dielectric material (a standard material). The MUT (with ground plane) is introduced to the top of the microstrip in order to

sandwich the transmission line thus creating a pseudo stripline structure. The test method involves conducting phase measurements to establish the change in phase ($\Delta\phi$) of the applied signal and corresponding change in the electrical length of the transmission line (Δl_e) before and after the application of the MUT. The phase and electrical length measurements are accomplished using an Anritsu MS46122B VNA. A sweep of two hundred measurements were performed using the VNA equipment and the average of the readings were taken for each MUT sample. The measured change in the electrical length can be used to establish the effective dielectric constant of the stripline (ϵ_{effs}). The value of ϵ_{effs} can then be used in conjunction with a calibration graph to obtain the ϵ_r of the MUT. For this work the calibration graph was generated by evaluating a simulation model of the testing rig for known values of ϵ_r . The simulation software used for the calibration was the COMSOL Multiphysics software. It is important to note that the accuracy of the test method is dependent on the MUT being securely clamped onto the surface of the standard substrate so as to eliminate any airgaps between the MUT and the transmission line.

2) TESTING SETUP

The test setup used for the two-layer stripline method is shown in Fig. 6. The first step in the construction of the testing rig was the design and manufacture of the standard dielectric substrate with the microstrip line. The standard material needed to have a known relative permittivity and was required to be outfitted with a 50 ohm microstrip line [9]. The chosen dielectric material for the standard layer of material was the Rogers Corporation 4350B laminate (double sided 0.5/0.5 oz copper, 1.524 mm substrate thickness, dielectric constant of 3.48 ± 0.05) [45]. The Rogers 4350B material was chosen because it provided a relatively constant value of dielectric constant across the test frequency band of 1 GHz to 10 GHz. The stated dielectric constant of the Rogers 4035B material (3.48) is also fairly similar to the stated dielectric constant of bulk PLA (2.75). For the two-layer stripline measurement method it is recommended that the dielectric constant of the MUT and the standard material are similar in order to reduce any large discontinuities at the microstrip line/stripline junction [9]. Using the COMSOL Multiphysics software and the RF toolbox, the microstrip line width was established for the Rogers substrate in order to achieve a 50 ohm impedance. The simulated microstrip line width of 3.43 mm was used. The manufacturing files required to produce the microstrip line were produced using the National Instruments Ultiboard PCB design software. The designed PCB was sized to be 200 mm \times 50 mm. The microstrip was subsequently manufactured by Sunstone PCB Ltd. The supplier also independently tested the impedance of the microstrip which was found to be 50.19 ohms. Finally, the microstrip was outfitted with SMA end launchers.

Once the known standard substrate with the 50 ohm microstrip line was produced it was necessary to manufacture the clamping jig for securing the known substrate and the

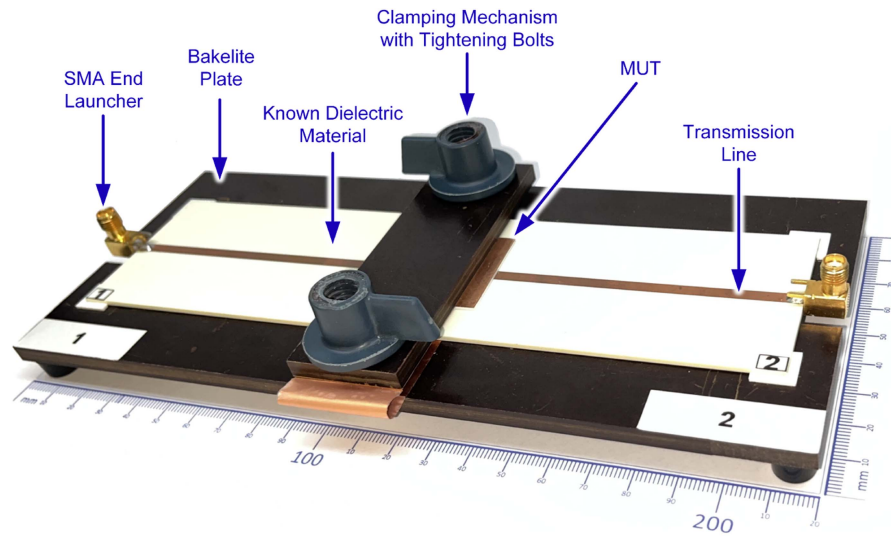


FIGURE 6. Details of the of the testing rig constructed for the two-layer stripline measurement method.

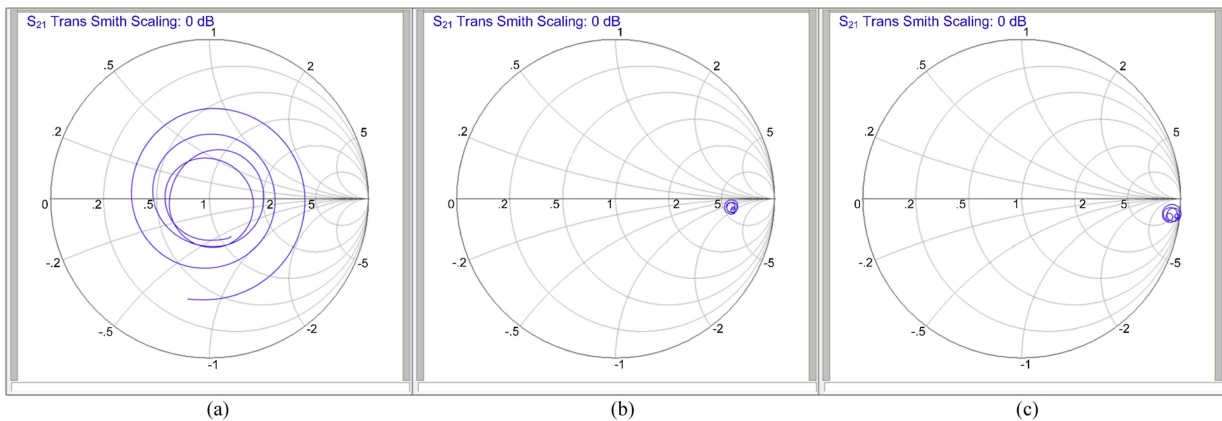


FIGURE 7. Example S_{21} locus plots for the two-layer stripline measurement method (a) locus plot of the stripline (b) locus plot of the stripline with an added electrical delay (c) locus plot of the microstrip only (no MUT) with an added electrical delay.

MUT samples. It is important that the clamp is able to provide a sufficient and even pressure to eliminate any air gaps between the MUT and the microstrip line. The material Bakelite was chosen for the construction of the clamp platform and clamping arm. Bakelite is a common insulator material that is easily machinable and provides a smooth surface with sufficient rigidity. The machined surface of the platform and clamping were provided with grounding connections to allow for the electrical connection of the microstrip line ground plane and the MUT ground plane. Finally, two nylon bolts with thumb screws were used to secure the clamping plate and the platform base.

3) TESTING PROCEDURE

The completed testing rig (with MUT and known substrate mounted) was connected to an Anritsu MS46122B VNA. With the MUT present, the transmission line becomes a pseudo stripline. A Smith chart locus plot of S_{21} is generated by the VNA equipment for a specified frequency sweep.

The frequency range of interests was 1 GHz to 10 GHz and frequency sweeps were performed in 1 GHz increment steps (10 MHz steps were used for each increment). For each test two hundred sweeps were performed and the measured data was averaged to obtain the final reading. Fig. 7(a) shows an example of the S_{21} locus plot of the two-layer stripline for a frequency sweep of 1 GHz to 2 GHz. The MUT in the example is a 3DP sample with the Zig-Zag infill pattern.

The VNA equipment allows for the introduction of an electrical delay to the reference plane. The introduction of the delay is reflected in a change in the Smith chart plot with the locus of S_{21} becoming tighter and shifted to the right of the $1.0\angle 0$. The value of the delay is noted. Fig. 7(b) shows an example of the S_{21} locus plot of the two-layer stripline for a frequency sweep of 1 GHz to 2 GHz with the introduction of the delay to the previous plot shown in Fig. 7(a). The MUT is then removed and the clamping arm opened leaving only the microstrip line. The impedance of the microstrip line is now different to the previous two-layer stripline configuration.

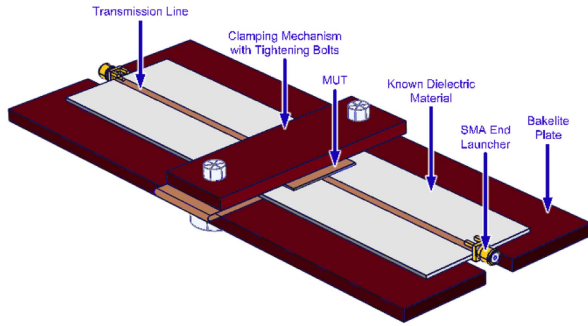


FIGURE 8. COMSOL Multiphysics simulation model of the two-layer stripline testing rig.

This change in impedance requires an adjustment to the electrical delay to reposition the S_{21} locus of the microstrip line. This new delay is also noted. Fig. 7(c) shows the S_{21} locus plot of the microstrip line with the Rogers 4035B substrate with a delay added for a frequency sweep of 1 GHz to 2 GHz.

Having obtained the electrical delay with and without the MUT the value for the change in electrical length Δl_e can be obtained. The measured $\Delta \tau_e$ is related to the effective dielectric constant of the stripline ϵ_{effs} by (16) [9]:

$$\epsilon_{effs} = \left(\sqrt{\epsilon_{effm}} + \frac{\Delta \tau_e \cdot \lambda_0}{l_p} \right)^2 \quad (16)$$

where λ_0 is the wavelength of the applied signal in free space, $l_p = 40.00$ mm which is the length of the MUT sample along the transmission line and ϵ_{effm} is the effective dielectric constant of the microstrip line. The value of ϵ_{effm} was obtained from (17) [46]:

$$\epsilon_{effm} = \frac{\epsilon_r + 1}{2} + \frac{\epsilon_r - 1}{2} \left[1 + 12 \left(\frac{H}{w} \right) \right]^{-\frac{1}{2}} \quad (17)$$

where the substrate is the Rogers Corporation 4350B laminate and $\epsilon_r = 3.48 \pm 0.05$, $H = 1.52 \pm 0.02$ mm, $w = 3.43 \pm 0.02$ mm and $\epsilon_{effm} = 2.73$.

4) SIMULATED CALIBRATION GRAPH

Having obtained the values of ϵ_{effs} from the measurement data the next required step would involve obtaining the dielectric constant (ϵ_r) of the MUT (the 3DP dielectric sample). The values can be obtained from the relevant calibration graph relating the values of ϵ_{effs} and ϵ_r [9]. The calibration graph was produced using an appropriate simulation model of the testing setup. Using the COMSOL Multiphysics software and the RF toolbox, a model of the testing rig was created. The simulation model is shown in Fig. 8. The model provides information on the phase constant of the transmission line (β) for various known test values of the relative permittivity (ϵ_r) of the MUT. The values of ϵ_{effs} are obtained for a given values of β from (18) [46]:

$$\epsilon_{effs} = \left(\frac{\beta c_0}{\omega} \right)^2 \quad (18)$$

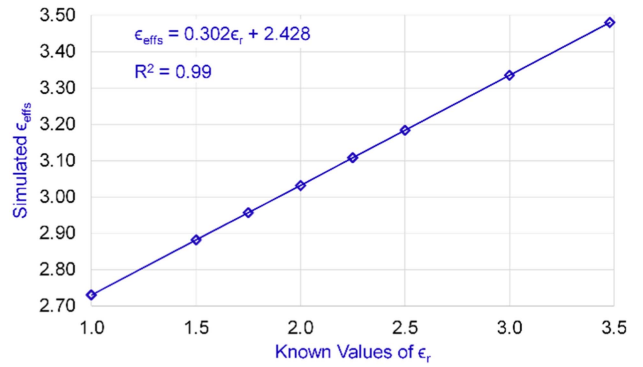


FIGURE 9. Calibration graph of ϵ_{effs} generated using the COMSOL Multiphysics software for assumed known values of dielectric permittivity (ϵ_r) of the 3DP samples (MUT).

TABLE 2. Details of the COMSOL Multiphysics Model Used to Obtain the Calibration Graph for the Measured Values of ϵ_{effs}

Assumed Known Values of ϵ_r	Simulated Values of ϵ_{effs}
1.00	2.730
1.50	2.882
1.75	2.957
2.00	3.031
2.25	3.108
2.50	3.184
3.00	3.335
3.50	3.486

Simulation Model Details	
Dielectric permittivity of standard material (ϵ_1)	3.48
Standard material thickness	1.52 mm
Microstrip line width	3.43 mm
3DP dielectric material thickness	0.80 mm

VI. CALCULATED AND MEASURED RESULTS

This section of the work presents the results obtained from the empirical study as well as the data obtained from the evaluated mixture models. The measured and estimated data will also be compared.

A. MEASURED ϵ_{eff} DATA FOR 3DP SAMPLES

Fig. 9 shows the calibration graph of ϵ_{effs} which was generated from the COMSOL Multiphysics simulations of the testing setup (as shown in Fig. 8) for assumed known values of ϵ_r . The derived equation for the data trendline is:

$$\epsilon_{effs} = 0.302\epsilon_r + 2.428 \quad (19)$$

The simulation model details are recorded in Table 2. All dimensions used in the simulation model were measured from the physical rig using a vernier calliper with an accuracy of 0.02 mm.

Table 3 shows the measured volume fraction (%vol) of PLA for the 3DP dielectric substrates for each infill pattern. The

TABLE 3. Measured ϵ_{effs} , ϵ_r and %vol of PLA for the 3DP Samples With Various Infill Patterns

Infill Pattern	%vol of PLA	Measured ϵ_{effs}	Measured ϵ_r
Octet	55.18%	3.024	1.97
Quarter Cubic	55.76%	3.026	1.98
Cubic Subdivision	57.07%	3.021	1.96
Cubic	57.61%	3.015	1.94
Concentric	57.76%	3.021	1.96
Lightening	58.37%	3.021	1.96
Grid	58.77%	3.016	1.95
Tri-hexagon	59.34%	3.016	1.95
Lines	59.38%	3.025	1.97
Triangles	59.74%	3.015	1.94
Cross 3D	60.14%	3.020	1.96
Gyroid	61.02%	3.021	1.96
Cross	61.24%	3.023	1.97
Zig-Zag	61.47%	3.024	1.97
Full	86.81%	3.133	2.33

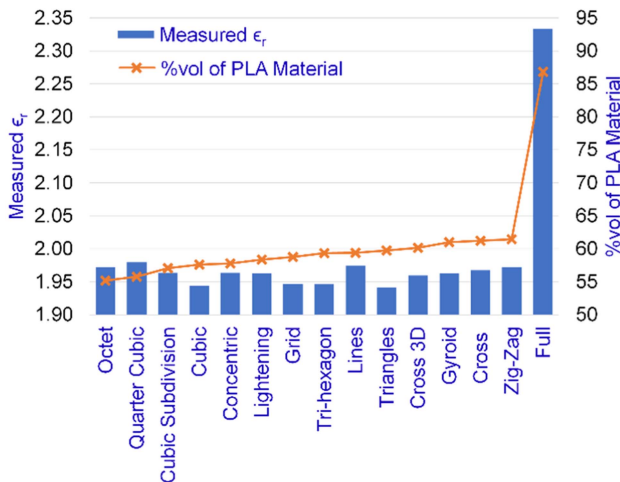


FIGURE 10. Comparative plot of the measured ϵ_r for the 3DP samples and the %vol of PLA for each sample.

values of ϵ_{effs} which were obtained from the measurements are also recorded. The table also records the measured values of ϵ_r for the 3DP material samples with various infill patterns as obtained from the calibration graph using the measured values of ϵ_{effs} . Fig. 10 provides a graphical plot of the measured data for the ϵ_r of the two-layer stripline for the MUT samples with various infill patterns. The data plot is superimposed against a plot of the data related to the %vol of PLA for each of the MUT samples. The measured values of ϵ_r did not track the variations in the %vol of the 3D printed dielectric samples.

For the range of values of measured ϵ_r recorded for the 3DP MUT samples there was a variation of 0.04 for the measured ϵ_r between the smallest recorded value (triangles infill) and largest values (quarter cubic infill). The changes in the measured ϵ_r did not follow the variation in the %vol of PLA in the samples. This implies that a factor other than the %vol

of material contained within the 3DP material mixture was affecting the dielectric constant of the material mixture.

1) ERROR ANALYSIS OF TWO-LAYER STRIPLINE MEASUREMENT METHOD

From (17), the error for the microstrip line constructed using the Rogers 4350B laminate (standard substrate material) can be expressed as:

$$\Delta\epsilon_{effm} = \sqrt{\left(\frac{\delta\epsilon_{effm}}{\delta\epsilon_r}\Delta\epsilon_r\right)^2 + \left(\frac{\delta\epsilon_{effm}}{\delta H}\Delta H\right)^2 + \left(\frac{\delta\epsilon_{effm}}{\delta w}\Delta w\right)^2} \quad (20)$$

and $\Delta\epsilon_{effm} = 0.05$.

Equation (16) provided an expression for ϵ_{effs} , the effective dielectric permittivity of the stripline. Therefore, the error for ϵ_{effs} can be expressed as:

$$\begin{aligned} \Delta(\sqrt{\epsilon_{effs}}) &= \Delta(\sqrt{\epsilon_{effm}}) + \Delta\left(\frac{\tau_e\lambda_0}{l_p}\right) \\ &= \frac{\Delta\epsilon_{effm}}{2\sqrt{\epsilon_{effm}}} + \frac{\Delta\tau_e\lambda_0}{l_p} + \frac{\Delta l_p\tau_e\lambda_0}{l_p^2} \end{aligned} \quad (21)$$

Ignoring the second order factor from (21) the expression can be simplified to:

$$\Delta(\sqrt{\epsilon_{effs}}) \approx \frac{\Delta\epsilon_{effm}}{2\sqrt{\epsilon_{effm}}} + \frac{\Delta\tau_e\lambda_0}{l_p} \quad (22)$$

and

$$\Delta(\sqrt{\epsilon_{effs}}) = \frac{\Delta\epsilon_{effs}}{2\sqrt{\epsilon_{effs}}} \approx \frac{\Delta\epsilon_{effm}}{2\sqrt{\epsilon_{effm}}} + \frac{\Delta\tau_e\lambda_0}{l_p} \quad (23)$$

Hence,

$$\Delta\epsilon_{effs} = \frac{\sqrt{\epsilon_{effs}}}{\sqrt{\epsilon_{effm}}}\Delta\epsilon_{effm} + \frac{2\Delta\tau_e\lambda_0\sqrt{\epsilon_{effs}}}{l_p} \quad (24)$$

With reference to the calibration graph shown in Fig. 9 and the expression given by (19) we can consider:

$$\Delta\epsilon_r \sim \Delta\epsilon_{effs}/0.302 \quad (25)$$

and therefore,

$$\Delta\epsilon_r = \left(\frac{\sqrt{\epsilon_{effs}}}{\sqrt{\epsilon_{effm}}}\Delta\epsilon_{effm} + \frac{2\Delta\tau_e\lambda_0\sqrt{\epsilon_{effs}}}{l_p}\right)/0.302 \quad (26)$$

A set of ten 3DP samples were produced for each infill pattern. The length of the 3DP samples is $l_p = 40$ mm. For a typical value of $\epsilon_{effs} = 3.02$ and assuming $\Delta\tau_e = 0.01$ mm, the error for the measured ϵ_r would be:

$$\Delta\epsilon_r = 0.01 \quad (27)$$

B. ESTIMATED ϵ_{eff} DATA FROM MIXTURE MODELS

This section presents the data obtained from the evaluation of the volume fraction and shape factor mixture models for

TABLE 4. Estimated Values of ϵ_{eff} for Various %vol Mixture Models for the 3DP Dielectric Samples

Infill pattern	%vol PLA	Estimated ϵ_{eff} for various %vol mixture models					Measured ϵ_r
		RAY	RI	BOT	LLL	LI	
Octet	55.18%	1.86	1.86	1.83	1.82	1.75	1.97
Quarter Cubic	55.76%	1.87	1.87	1.84	1.83	1.76	1.98
Cubic Sub.	57.07%	1.90	1.89	1.86	1.86	1.78	1.96
Cubic	57.61%	1.90	1.90	1.87	1.87	1.79	1.94
Concentric	57.76%	1.91	1.91	1.87	1.87	1.79	1.96
Lightening	58.37%	1.92	1.92	1.89	1.88	1.80	1.96
Grid	58.77%	1.93	1.92	1.89	1.89	1.81	1.95
Tri-hexagon	59.34%	1.94	1.93	1.90	1.90	1.82	1.95
Lines	59.38%	1.94	1.93	1.91	1.90	1.82	1.97
Triangles	59.74%	1.94	1.94	1.91	1.90	1.83	1.94
Cross 3D	60.14%	1.95	1.95	1.92	1.91	1.84	1.96
Gyroid	61.02%	1.97	1.96	1.94	1.93	1.85	1.96
Cross	61.24%	1.97	1.97	1.94	1.93	1.86	1.97
Zig-Zag	61.47%	1.97	1.97	1.95	1.94	1.86	1.97
Full	86.81%	2.47	2.47	2.46	2.45	2.41	2.33

the various 3DP dielectric samples. The %vol of PLA for the samples was as calculated from (1) using the measured weight of the samples.

1) VOLUME FRACTION (%VOL) MIXTURE MODELS

Table 4 shows the calculated values of ϵ_{eff} for the RAY, RI, BOT, LLL, and LI volume fraction mixture models respectively for the measured values of %vol of PLA for the 3DP samples with various infill patterns. For all the mixture models, the predicted ϵ_{eff} was observed to increase with an increase in the %vol of PLA. For each value of the %vol of PLA, the predicted value for the RAY model was highest followed by the RI, BOT, LLL, and LI in decreasing order of magnitude.

Fig. 11 shows the plot of the value of ϵ_{eff} as predicted by the volume fraction mixture models as well as the data measured using the two-layer stripline measurement method. Significant variation was observed between the measured and predicted values of ϵ_{eff} for several of the infill patterns. The octet, quarter cubic, cubic subdivision, cubic, concentric, lightening, and lines infill patterns all had measured values higher than those predicted by the volume fraction mixture models. On the other hand, the predicted value was greater than the measured value for the 100% infill (full) printed sample. The grid, tri-hexagon, triangles, cross 3D, gyroid, cross, and zig-zag mixture models demonstrated close agreement between the measured value for these infill patterns and the RI and RAY models. The BOT, LLL, and LI mixture models did not provide predicted values of ϵ_{eff} which were able to closely match any of the measure data for the various infill patterns.

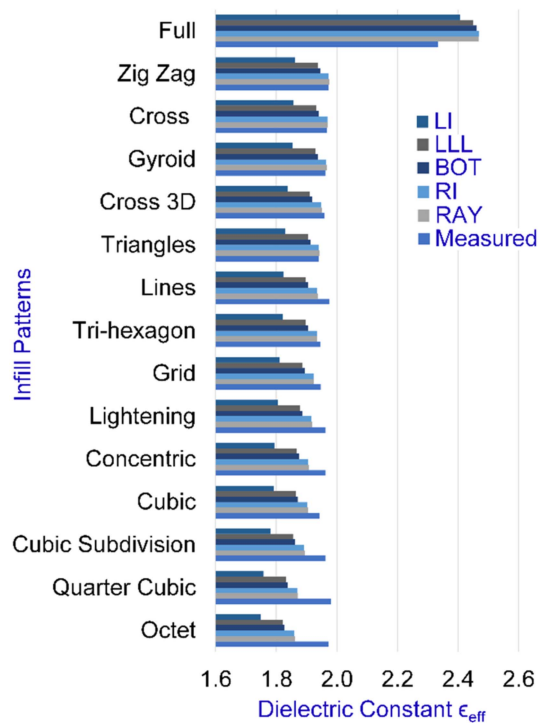


FIGURE 11. Plot of the measured and predicted values of ϵ_{eff} for the various infill patterns of the 3DP samples for the volume fraction mixture models.

TABLE 5. MSE for the Various %vol Mixture Models

MM	RAY	RI	BOT	LLL	LI
MSE	3.66×10^{-3}	3.89×10^{-3}	6.74×10^{-3}	7.39×10^{-3}	2.23×10^{-2}

The Mean Squared Error (MSE) was calculated for the values of ϵ_{eff} which were predicted by the various %vol mixture models. The MSE was chosen to give a quantitative measure of the degree to which the estimated values deviate from the measured data. The MSE values for the volume fraction mixture models (MM) are shown in Table 5. The calculated value of MSE was lowest for the RAY mixture model with an increased MSE for the RI, BOT, LLL, and LI in that order. The MSE for the RAY and RI models were fairly close with a difference of 0.23×10^{-3} . The BOT and LLL models were similarly close with a difference of 0.64×10^{-3} . In considering the MSE values it is important to be cognisant of the fact that the volume fraction mixture models only give consideration to the volume of materials contained within the mixture. Therefore, the MSE values allow for a measure of how well the volume fraction mixtures are able to estimate the values of ϵ_{eff} based solely on the changing %vol of PLA in each 3DP sample.

2) SHAPE FACTOR MIXTURE MODELS

Table 6 shows the calculated values of ϵ_{eff} for the SF and EMT mixture models respectively for the measured values of

TABLE 6. Estimated Values of ϵ_{eff} for Various Shape Factor Mixture Models for the 3DP Dielectric Samples

Infill pattern	%vol PLA	Estimated ϵ_{eff} for various %vol mixture models			Measured ϵ_r
		SF-Inc	SF-Per	EMT	
Octet	55.18%	1.54	1.22	2.24	1.97
Quarter Cubic	55.76%	1.55	1.23	2.25	1.98
Cubic Sub.	57.07%	1.57	1.23	2.26	1.96
Cubic	57.61%	1.58	1.23	2.26	1.94
Concentric	57.76%	1.58	1.23	2.27	1.96
Lightening	58.37%	1.59	1.23	2.27	1.96
Grid	58.77%	1.60	1.23	2.28	1.95
Tri-hexagon	59.34%	1.61	1.24	2.28	1.95
Lines	59.38%	1.61	1.24	2.28	1.97
Triangles	59.74%	1.61	1.24	2.29	1.94
Cross 3D	60.14%	1.62	1.24	2.29	1.96
Gyroid	61.02%	1.63	1.24	2.30	1.96
Cross	61.24%	1.64	1.24	2.30	1.97
Zig-Zag	61.47%	1.64	1.24	2.30	1.97
Full	86.81%	2.23	1.32	2.59	2.33

TABLE 7. MSE for the Various %vol Mixture Models

MM	EMT	SF-Inc	SF-Per
MSE	9.78×10^{-2}	1.25×10^{-1}	5.62×10^{-1}

%vol of PLA for the 3DP samples with various infill patterns. For all the mixture models, the predicted ϵ_{eff} was observed to increase with an increase in the %vol of PLA. For each value of the %vol of PLA, the predicted value for the EMT model was highest followed by the SF-Inc and SF-Per in decreasing order of magnitude.

Fig. 12 shows the plot of the value of ϵ_{eff} as predicted by the shape factor mixture models as well as the data measured using the two-layer stripline measurement method. None of the shape factor mixture models were able to provide estimated values of ϵ_{eff} which corresponded to the measured values. The EMT model estimated values exceeded the measured value of ϵ_{eff} for all the infill samples. On the other hand, the estimated values of ϵ_{eff} for the SF-Per and SF-Inc mixture models were all below the measured value of ϵ_{eff} for the various infill patterns.

The Mean Squared Error (MSE) was calculated for the values of ϵ_{eff} which were predicted by the various shape factor mixture models (MM) and are shown in Table 7.

The calculated value of MSE was lowest for the EMT mixture model with an increased MSE for the SF-Inc and SF-Per models in that order.

VII. ANALYSIS AND DISCUSSIONS

This section of the work discusses the results obtained from the empirical study. The fit of the %vol and shape factor

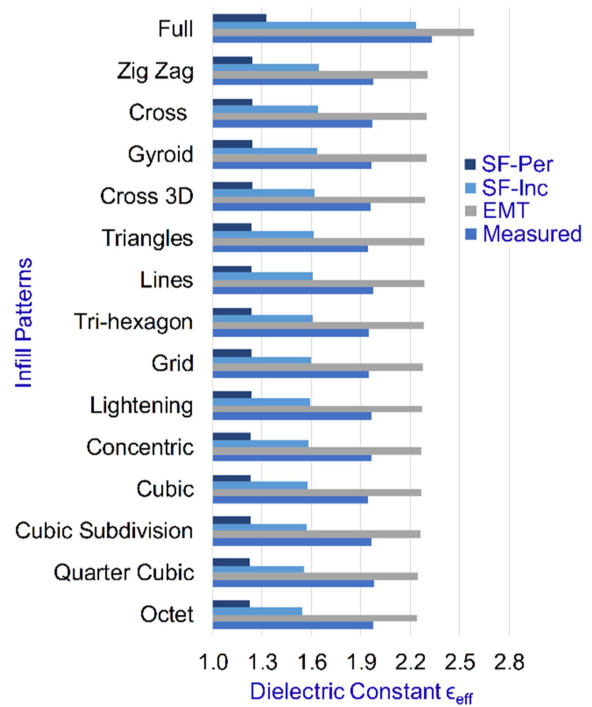



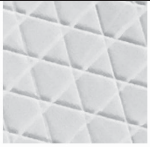
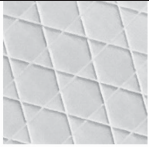




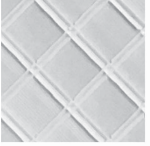
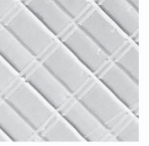




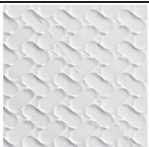
FIGURE 12. Plot of the measured ϵ_r for the 3DP samples with varying infill patterns and the predicted ϵ_{eff} for the shape factor mixture models.

mixture models for estimating the dielectric constant of the 3DP dielectric substrates is also discussed.

A. DETAILS OF INFILL PATTERNS AND MEASURED DIELECTRIC CONSTANT

The measured data has shown that the variation in ϵ_r for the binary 3DP samples do not directly correlate to the increase in the %vol of the PLA in the samples. Table 8 illustrates and discusses the observed results and the construction of the 3DP samples. The measured data for ϵ_r for the 3DP samples presents several points of interest. From the measured data, several infill patterns demonstrated higher values of ϵ_r for the measured data but also possessed low %vol values for the measured range of %vol values. An example of this is the octet infill with a %vol and ϵ_r of 55.18% and 1.97 respectively compared to the zig-zag infill with values of 61.47% and 1.97 respectively. The difference in %vol for the two samples translates into a weight difference of 6.29% (0.08 g). Therefore, a change in infill pattern can help with weight reduction without a change in the value of ϵ_r . Similarly, a change in pattern can allow for a variation in the resultant ϵ_r for similar material consumption. An example of this is the lines and triangles infill pattern with a difference in %vol of 0.36% (0.004 g) and a $\Delta\epsilon_r$ of 0.03. Finally, an infill pattern can be chosen which can provide a secondary benefit (for example, increased flexibility, increased rigidity in all three axes etc.) without a resultant change in the value of ϵ_r . An example would be the concentric infill which is described as allowing flexibility in a 3D model and lightening which allows for rapid

TABLE 8. Relevant Details of the Infill Patterns for the 3DP Samples

		
Triangles $\epsilon_r = 1.94$	Cubic $\epsilon_r = 1.94$	Tri-hexagon $\epsilon_r = 1.95$
	Triangles, cubic and tri-hexagon all share a similar triangular structure with cubic and tri-hexagon having a more star structure. The measured values of ϵ_r were equal for triangles and cubic with tri-hexagon having a slightly higher value and cubic-subdivision having the highest value of ϵ_r with an overall difference of 0.02.	
Cubic-subdivision $\epsilon_r = 1.96$		
		
Grid $\epsilon_r = 1.95$	Zig-Zag $\epsilon_r = 1.97$	Lines $\epsilon_r = 1.97$
Grid, zig-zag and lines infill all share a similar diamond pattern with zig-zag and lines having similar densities and similar values of ϵ_r . Grid which has a density that is approximately one quarter that of the other two patterns has a smaller value of ϵ_r with an overall difference of 0.02.		
		Octet and quarter cubic have a diamond pattern with quarter cubic having twice the density. Octet has double walls along both diagonals while quarter cubic only has along one. There is an overall difference of 0.01 for the measured ϵ_r .
Octet $\epsilon_r = 1.97$	Quarter cubic $\epsilon_r = 1.98$	
		Cross 3D and cross both create long pathways cutting across the infill diagonally that are free of obstructions. Cross is denser and there is an overall difference of 0.01 for the measured ϵ_r .
Cross 3D $\epsilon_r = 1.96$	Cross $\epsilon_r = 1.97$	
		
Concentric $\epsilon_r = 1.96$	Lightening $\epsilon_r = 1.96$	Gyroid $\epsilon_r = 1.96$
Concentric, lightening, and gyroid are unique infills which are significantly different from each other in structure. Concentric produces infill lines which are parallel to the external walls of the 3DP dielectric structure. Lightening is designed to be random/chaotic and gyroid is constructed of pill shaped cells aligned diagonally. The measured values of ϵ_r for all three infill patterns were the same.		

printing but with lowered strength [40]. Both infill patterns provide the same ϵ_r with varying mechanical properties.

While we have discussed the possible design freedom in constructing the 3D printed dielectric substrate with various infill pattern options it is also worth highlighting that the choice of infill pattern can have an impact on applications that are sensitive to the accuracy of the dielectric constant value. One example application area would be sensor design. In our

previous work we have examined the impact of the variations of the substrate dielectric constant on the performance of a complementary split ring resonator (CSRR) topology for non-invasive blood glucose and creatine monitoring [7]. The performance parameters examined were the resonant frequency and reflection coefficient (S_{11}). The variations in the dielectric constant which were examined were <0.08 . The maximum variation in the resonant frequency was 1.25 GHz and the 1.5 dB for S_{11} . This example is sufficiently sensitive to the change in the dielectric constant of the substrate such that the differences in the dielectric constant based on the infill patterns will affect the sensor performance.

B. COMPARISON OF MIXTURE MODEL ϵ_{eff} ESTIMATES AND MEASURED ϵ_r

For the 3DP samples none of the shape factor mixture models were able to provide good estimates of the measured values of permittivity. The poor fit was shown by the high MSE values for the various shape factor mixture models when compared to the measured data. For the volume fraction mixture models, some models were able to provide fairly close estimates of the measured permittivity for specific infill patterns. Overall, the volume fraction mixture models provided better estimates as shown by the lower MSE values when compared to the shape factor mixture models.

VIII. CONCLUSION

Several volume factor models were identified and evaluated for binary mixtures of 3DP material (PLA) and air. The volume fraction models included the Landau & Lifshitz, Looyenga (LLL), Rayleigh (RAY), Refractive Index (RI), Lichtenecker (LI), and Böttcher (BOT) models. The models were found to possess a wide variation in the predicted values of dielectric permittivity for a given %vol of material. Several shape factor models were also identified and evaluated for binary mixtures of PLA and air. The shape factor mixture models included the Sillars & Fricke (SF) and Emets (EMT) models where the SF model considered two boundary conditions of the applied field being incident (SF-Inc) and perpendicular (SF-Per) to the 3DP lines or material. The shape factor mixture models were considered to be relevant to the 3DP dielectric structures for the condition where the discontinuities within the 3DP structure were such that the material mixture could no longer be considered to be homogenous. The presence of infill patterns within the 3DP structure presented suitable conditions for the realization of discontinuities within the 3DP substrate which could potentially have an impact on the applied signal field. The shape factor mixture models were also seen to provide a wide variation in the predicted values of dielectric permittivity of a given %vol and infill pattern.

The identified material mixture models were then compared with measured values of dielectric permittivity from prepared 3DP dielectric samples. 3DP samples were prepared with fixed %infill (10%) and various infill patterns. The samples allowed for the evaluation of the impact of changes to the infill pattern on the dielectric constant of the 3DP structure.

The two-layer stripline measurement method was selected for this research and allowed for the rapid testing of multiple samples. The measured dielectric constant for the samples with fixed %infill and varying infill patterns did not show a similar increase in measured data as the %vol of PLA material in the 3DP samples increased. This result suggests that the change in the infill pattern of the 3DP material mixtures did impact the resultant dielectric permittivity of the 3DP electrical structure. The comparison of the measured data for the 3DP dielectric samples with varying infill patterns and the shape factor mixture models did not find any close agreement between the models and the measured data. The calculated MSE for the shape factor mixture models was best overall for the EMT model. However, improved fit was noted on a case by case basis for each infill. For example, for the 100% infill dielectric sample, the best estimation was provided by the SF-Inc shape factor mixture model. The comparison of the measured data for the 3DP dielectric sample with varying infill patterns and the %vol mixture models found improved agreement between the estimated values and the measured data. The calculated MSE for the shape factor mixture models was lowest for the RAY model. On an individual basis, various infill patterns showed good agreement with specific volume fraction mixture models. Examples of this included the zig-zag, cross, gyroid, and triangles infill patterns with the RI mixture model.

IX. FUTURE WORK

The results from this research have shown that for 3DP material mixtures, factors in addition to the percentage volume composition of the materials would impact the resultant dielectric permittivity of the electrical structure. Specifically, the choice of the infill pattern of the 3DP electrical structure can directly impact the resultant dielectric permittivity. The various infill patterns that were examined in this work were all produced using a 10% infill. Detailed studies of each infill pattern with a suitably wide variation in the %infill of the 3D printed materials can be undertaken to examine the ability of the mixture models to predict the dielectric constant of the materials. The present work was limited to binary material mixtures and also the testing frequency range. Future work can allow for the investigation of higher order material mixture models. This is particularly relevant for applications which involve the exposure of the 3DP electrical structure to moisture and other contaminants. The ingress of material into the infill pattern can potentially result in changes to the EM properties of the 3DP material mixture. The deliberate doping of sections of the infill pattern cavities can also be investigated in order to create novel dielectric materials. In addition, extending the frequency range of testing higher would allow for the introduction of increased anisotropic responses as relates to the geometric discontinuities within the 3DP substrate structure and the wavelength of the applied signal. Finally, the dielectric substrates examined in this work were constructed using FFF 3DP. Dielectric substrates with the same infill patterns can be constructed using different 3DP

technologies (such as material jetting) to investigate the impact of the 3DP process on the resultant dielectric constant of the 3D printed material mixture.

REFERENCES

- [1] T. Altenburg, "Sustainable Global Supply Chains Report 2022," IDOS: German Institute of Development and Sustainability, Bonn, Germany, 2022. [Online]. Available: <https://policycommons.net/artifacts/3346290/sustainable-global-supply-chains-report-2022/4145190/>
- [2] D. Shawn, "The current sentiment of the global electronics manufacturing supply chain," IPC, Bannockburn, IL, USA, 2022. [Online]. Available: <https://emails.ipc.org/links/0422CurrentSentimentGlobal-EMSC-IPC.pdf>
- [3] J. Persad and S. Rocke, "A survey of 3D printing technologies as applied to printed electronics," *IEEE Access*, vol. 10, pp. 27289–27319, 2022.
- [4] J. Persad and S. Rocke, "Multi-material 3D printed electronic assemblies: A review," *Results Eng.*, vol. 16, 2022, Art. no. 100730.
- [5] A. H. Espera, J. R. C. Dizon, Q. Chen, and R. C. Advincula, "3D-printing and advanced manufacturing for electronics," *Prog. Additive Manuf.*, vol. 4, pp. 245–267, 2019.
- [6] E. Tuncer and S. M. Gubanski, "Dielectric properties of different composite structures," *Polym. Liquid Crystals*, vol. 4017, pp. 136–142, 1999.
- [7] J. Persad, S. Rocke, A. Roopnarine, and A. Abdool, "Investigating the impact of substrate composition on 3D printed mmWave CSRR sensor," in *Proc. COMSOL Conf. North Amer.*, 2020.
- [8] J. Coonrod, "Characterizing circuit materials at mmWave frequencies: Part I," *mmWave Des. Guide*, vol. 62, no. 10, Oct. 2019, Art. no. 14.
- [9] N. K. Das, S. M. Voda, and D. M. Pozar, "Two methods for the measurement of substrate dielectric constant," *IEEE Trans. Microw. Theory Techn.*, vol. 35, no. 7, pp. 636–642, Jul. 1987.
- [10] M. Ansari, O. Zetterstrom, N. J. Fonseca, O. Quevedo-Teruel, and Y. J. Guo, "A lightweight spherical generalized Luneburg lens antenna with low cross-polarization over a wide range in azimuth and elevation," *IEEE Open J. Antennas Propag.*, vol. 5, no. 1, pp. 58–66, Feb. 2024.
- [11] S. Zhang, R. K. Arya, S. Pandey, Y. Vardaxoglou, W. Whittow, and R. Mittra, "3D-printed planar graded index lenses," *IET Microw., Antennas Propag.*, vol. 10, no. 13, pp. 1411–1419, 2016.
- [12] C. Wang, J. Wu, and Y.-X. Guo, "A 3-D-printed wideband circularly polarized parallel-plate Luneburg lens antenna," *IEEE Trans. Antennas Propag.*, vol. 68, no. 6, pp. 4944–4949, Jun. 2020.
- [13] N.-A. A. B. Taib et al., "A review on poly lactic acid (PLA) as a biodegradable polymer," *Polym. Bull.*, vol. 80, no. 2, pp. 1179–1213, 2023.
- [14] Standard Terminology for Additive Manufacturing Technologies-General Principles-Terminology, Standard I.A. 52900, ASTM, West Conshohocken, PA, USA, 2021.
- [15] M. Venkatesh and G. Raghavan, "An overview of microwave processing and dielectric properties of agri-food materials," *Biosyst. Eng.*, vol. 88, no. 1, pp. 1–18, 2004.
- [16] E. Tuncer, Y. V. Serdyuk, and S. M. Gubanski, "Dielectric mixtures: Electrical properties and modeling," *IEEE Trans. Dielectrics Elect. Insul.*, vol. 9, no. 5, pp. 809–828, Oct. 2002.
- [17] S. O. Nelson and S. Trabelsi, "Dielectric spectroscopy of wheat from 10 MHz to 1.8 GHz," *Meas. Sci. Technol.*, vol. 17, no. 8, 2006, Art. no. 2294.
- [18] E. Tuncer, "Dielectric mixtures-importance and theoretical approaches," *IEEE Elect. Insul. Mag.*, vol. 29, no. 6, pp. 49–58, Nov./Dec. 2013.
- [19] M. Kurtinec, R. Hamar, and J. Pihera, "Complex permittivity models of composite dielectrics," in *Proc. IEEE Int. Conf. Solid Dielectrics*, 2007, pp. 39–42.
- [20] J. Persad and S. Rocke, "Investigating the impact of deformation on a 3D-printed antenna in Biomedical systems," *West Indian J. Eng.*, vol. 42, no. 2, pp. 66–76, 2020.
- [21] R. Garrappa, F. Mainardi, and M. Guido, "Models of dielectric relaxation based on completely monotone functions," *Fractional Calculus Appl. Anal.*, vol. 19, no. 5, pp. 1105–1160, 2016.

- [22] Y. Feldman, T. Skodvin, and J. Sjöblom, *Dielectric Spectroscopy on Emulsion and Related Colloidal Systems—A Review*. New York, NY, USA: Marcel Dekker, 2001.
- [23] E. Tuncer, S. M. Gubański, and B. Nettelblad, “Dielectric relaxation in dielectric mixtures: Application of the finite element method and its comparison with dielectric mixture formulas,” *J. Appl. Phys.*, vol. 89, no. 12, pp. 8092–8100, 2001.
- [24] H. Looyenga, “Dielectric constants of heterogeneous mixtures,” *Physica*, vol. 31, no. 3, pp. 401–406, 1965.
- [25] J. Widjajakusuma, B. Biswal, and R. Hilfer, “Quantitative comparison of mean field mixing laws for conductivity and dielectric constants of porous media,” *Physica A, Stat. Mechanics Appl.*, vol. 318, no. 3/4, pp. 319–333, 2003.
- [26] B. M. Tareev, *Physics of Dielectric Materials*. Moscow, Russia: Mir, 1975.
- [27] J. R. Birchak, C. G. Gardner, J. E. Hipp, and J. M. Victor, “High dielectric constant microwave probes for sensing soil moisture,” *Proc. IEEE*, vol. 62, no. 1, pp. 93–98, Jan. 1974.
- [28] K. Lichtenecker, “The dielectric constant of natural and artificial mixed bodies,” *Phys. J.*, vol. 27, pp. 115–158, 1926.
- [29] L. Rayleigh, “LVI. On the influence of obstacles arranged in rectangular order upon the properties of a medium,” *London, Edinburgh, Dublin Philos. Mag. J. Sci.*, vol. 34, no. 211, pp. 481–502, 1892.
- [30] S. O. Nelson, “Density-permittivity relationships for powdered and granular materials,” *IEEE Trans. Instrum. Meas.*, vol. 54, no. 5, pp. 2033–2040, Oct. 2005.
- [31] C. Böttcher, “The dielectric constant of crystalline powders,” *Recueil des Travaux Chimiques des Pays-Bas*, vol. 64, no. 2, pp. 47–51, 1945.
- [32] M. A. Scheller, S. Wietzke, C. Jansen, D. M. Mittleman, and M. Koch, “Heterogeneous dielectrics in the lower terahertz frequency range: Evaluation and extension of physical models,” in *Proc. Joint 32nd Int. Conf. Infrared Millimeter Waves 15th Int. Conf. THz Electron.*, 2007, pp. 542–543.
- [33] B. Sareni, L. Krähenbühl, A. Beroual, and C. Brosseau, “Effective dielectric constant of random composite materials,” *J. Appl. Phys.*, vol. 81, no. 5, pp. 2375–2383, 1997.
- [34] M. W. Elsallal, J. Hood, I. McMichael, and T. Busbee, “3D Printed material characterization for complex phased arrays and metamaterials,” *Microw. J.*, vol. 59, no. 10, pp. 20–34, Oct. 2016.
- [35] P. Steeman and F. Maurer, “An interlayer model for the complex dielectric constant of composites,” *Colloid Polym. Sci.*, vol. 268, pp. 315–325, 1990.
- [36] R. Sillars, “The properties of a dielectric containing semiconducting particles of various shapes,” *J. Inst. Elect. Engineers*, vol. 80, no. 484, pp. 378–394, 1937.
- [37] H. Fricke, “A mathematical treatment of the electric conductivity and capacity of disperse systems I. The electric conductivity of a suspension of homogeneous spheroids,” *Phys. Rev.*, vol. 24, no. 5, 1924, Art. no. 575.
- [38] Y. P. Emets, “Electrical characteristics of three-component dielectric media,” *J. Exp. Theor. Phys.*, vol. 87, no. 3, pp. 612–620, 1998.
- [39] *ANSI/NEMA Industrial Laminating Thermosetting Products*, Standard 60000-2021, National Electrical Manufacturers Association, Rosslyn, VA, USA, Nov. 2021.
- [40] U. Cura, *Ultimaker Cura Print Settings - Infill Settings*. New York, NY, USA: Ultimaker Cura, 2022.
- [41] Hatchbox, “Hatchbox PLA 3D printer filament,” Hatchbox, Pomona, CA, USA, 2016, pp. 1–3. [Online]. Available: https://cdn.shopify.com/s/files/1/0008/2457/4018/files/HATCHBOX_PLA_3D_Printer_Filament_SDS.pdf?1561
- [42] J. Krupka, R. N. Clarke, O. C. Rochard, and A. P. Gregory, “Split post dielectric resonator technique for precise measurements of laminar dielectric specimens—measurement uncertainties,” in *Proc. 3rd Int. Conf. Microw., Radar Wireless Commun. (MIKON)*, 2000, pp. 305–308.
- [43] K. C. Yaw, “Measurement of dielectric material properties application note,” Rohde & Schwarz, Changi, Singapore, 2018. [Online]. Available: https://cdn.rohde-schwarz.com/pws/dl_downloads/dl_application/00aps_undefined/RAC-0607-0019_1_5E.pdf
- [44] M. D. Janezic and J. A. Jargon, “Complex permittivity determination from propagation constant measurements,” *IEEE Microw. Guided Wave Lett.*, vol. 9, no. 2, pp. 76–78, Feb. 1999.
- [45] C. Rogers, “RO4000 series high frequency circuit materials,” Rogers Corporation, Chandler, AZ, USA, 2022. [Online]. Available: <https://rogerscorp.com/-/media/project/rogerscorp/documents/advanced-electronics-solutions/english/data-sheets/ro4000-laminates-ro4003c-and-ro4350b---data-sheet.pdf>
- [46] D. M. Pozar, *Microwave Engineering*. Hoboken, NJ, USA: Wiley, 2012.



JEEVAN PERSAD (Member, IEEE) received the B.Sc. degree in electrical and computer engineering from the University of the West Indies, Saint Augustine, Trinidad and Tobago in 2003, and the master’s degree in electronic product development from the University of Bolton, Bolton, U.K., in 2012. He is currently working toward the Ph.D. degree in electrical and computer engineering with the University of the West Indies. His research interests include the application of 3D printing to the manufacture of electronic assemblies.



SEAN ROCKE (Senior Member, IEEE) received the B.Sc. degree in electrical and computer engineering from the University of the West Indies, Saint Augustine, Trinidad and Tobago in 2002, the master’s degree in communications management and operational communications from Coventry University, Coventry, U.K., in 2004, and the Ph.D. degree in electrical and computer engineering from Worcester Polytechnic Institute, Worcester, MA, USA, in 2013. His research interests include statistical signal processing and optimization techniques

relating to wireless communications systems, and biosensor development and biomedical signal processing systems.